Electronic Supplementary Information

Photophysical Study on the Sequential Ion Interaction of an Organic Receptor: Optical Detection and Advanced Multifunctional Logic Applications.

Chinmoy Mahapatra,[a] Saikat Samanta,[b] Provakar Paul,[b] Indrani Ray Chowdhury,[c] Rajarshi Ghosh,[c] Arunavo Chatterjee,[d] Suvendu Paul,*[b] Tapas Majumdar*[b] and Arabinda Mallick*[a]

[a]Department of Chemistry, Kazi Nazrul University, Asansol, West Bengal, India – 713340. E-mail: ampcju@yahoo.co.in

[b]Department of Chemistry, University of Kalyani, Nadia, West Bengal, India – 741235. E-mail: paul.suvendu2016@gmail.com; tapasmju@gmail.com

[c]Department of Chemistry, The University of Burdwan, Burdwan, West Bengal, India – 713104.

[d]Department of Chemical Sciences, Indian Institute of Science Education and Research (IISER)–Kolkata, Mohanpur, West Bengal, India – 741246.

Contents

Table S1: Sensor information table containing the fluorescent probes that detected both Cu^{2+} & Zn^{2+} ions.

Ions detected	Fl. response	LOD for Zn^{2+}	LOD for Cu^{2+}	Medium	Ref.
Cu^{2+} & Zn^{2+}	Turn off (Cu^{2+}); Ratiometric (Zn^{2+})	……	……	HEPES buffered CH_3CN:H_2O (4:1; v/v) (pH= 7.0±0.1)	S1
Cu^{2+}, Zn^{2+} & F^-	Turn on (Zn^{2+} & F^-)	……	……	HEPES buffered MeOH:H_2O (pH= 7.2)	S2
Cu^{2+}, Zn^{2+}, Cd^{2+}, $H_2PO_4^-$, & PPi	Turn on (Zn^{2+}/Cd^{2+}) followed by turn off ($H_2PO_4^-$ & PPi)	650 nM	……	HEPES buffered MeOH:H_2O (pH= 7.3)	S3
Cu^{2+} & Zn^{2+}	Turn on (Zn^{2+})	10 µM	10 µM	CH_3CN	S4
Cu^{2+} & Zn^{2+}	Turn off (Cu^{2+}); Turn on (Zn^{2+})	19.4 nM	1.87 nM	HEPES buffered CH_3CN:H_2O (pH= 7.2)	S5
Cu^{2+} & Zn^{2+}	Turn on Zn^{2+} followed by turn off Cu^{2+}	31.04 nM	11.6 nM	HEPES buffered CH_3CN:H_2O (pH= 7.2)	S6
Cu^{2+} & Zn^{2+}	Turn off (Cu^{2+}); Turn on (Zn^{2+})	……	12.9 nM	CH_3CN	S7
Cu^{2+} & Zn^{2+}	Turn off (Cu^{2+}); Turn on (Zn^{2+})	911 nM	774 nM	EtOH/HEPES (Zn^{2+}) & THF/HEPES (Cu^{2+}); (pH =7.4)	S8
Cu^{2+} & Zn^{2+}	Turn on (Zn^{2+}) followed by turn off (Cu^{2+})	35 nM	1.46 µM	HEPES buffered CH_3CN:H_2O (pH= 7.2)	S9
Co^{2+}, Cu^{2+} & Zn^{2+}	Turn on (Zn^{2+})	37.0 nM	34.3 nM	HEPES buffered DMF:H_2O (pH= 7.0)	S10
Co^{2+}, Ni^{2+}, Cu^{2+} & Zn^{2+}	Turn on (Zn^{2+})	109 nM	623 nM	EtOH/tris- HCl buffer (pH=7.4)	S11
Zn^{2+} & NO	Turn on (Zn^{2+}) followed by turn off (NO)	9.94 nM	……	DMF/HEPES (3:7, v/v, pH = 7.4)	S12
Cu^{2+}	Turn on (Cu^{2+})	……	31 nM	PBS (pH= 7.4, 1% DMSO)	S13
Zn^{2+} & HOCl	Dual emission channel, Turn on (Zn^{2+}) & turn off (HOCl)	13.0 nM	……	PBS buffer (pH= 5.5)	S14
Cu^{2+} & S^{2-}	Turn off (Cu^{2+}) followed by turn on(S^{2-})	……	38.9 nM	HEPES buffered (pH= 7.4)	S15
Cu^{2+}	Turn off (Cu^{2+})	……	1.29 µM	30% CH_3CN in PBS (pH = 7.4)	S16
Cu^{2+} & NO_2^-	Turn off (Cu^{2+} & NO_2^-)	……	84 µM	CH_3CN & PBS (2:1, pH = 7.4)	S17
Zn^{2+}, Al^{3+} & F^-	Turn on (Zn^{2+}; & Al^{3+}); Turn off F^-	62.9 nM	……	MeOH	S18
Zn^{2+}, Cu^{2+} & $_2PO_4^-$	Turn on (Zn^{2+})	4.2 ppb	7.2 ppb	CH_3CN	S19
Cu^{2+} & Zn^{2+}	Turn on (Zn^{2+}) followed by turn off (Cu^{2+})	3.63 µM	5.69 µM	CH_3CN	This work

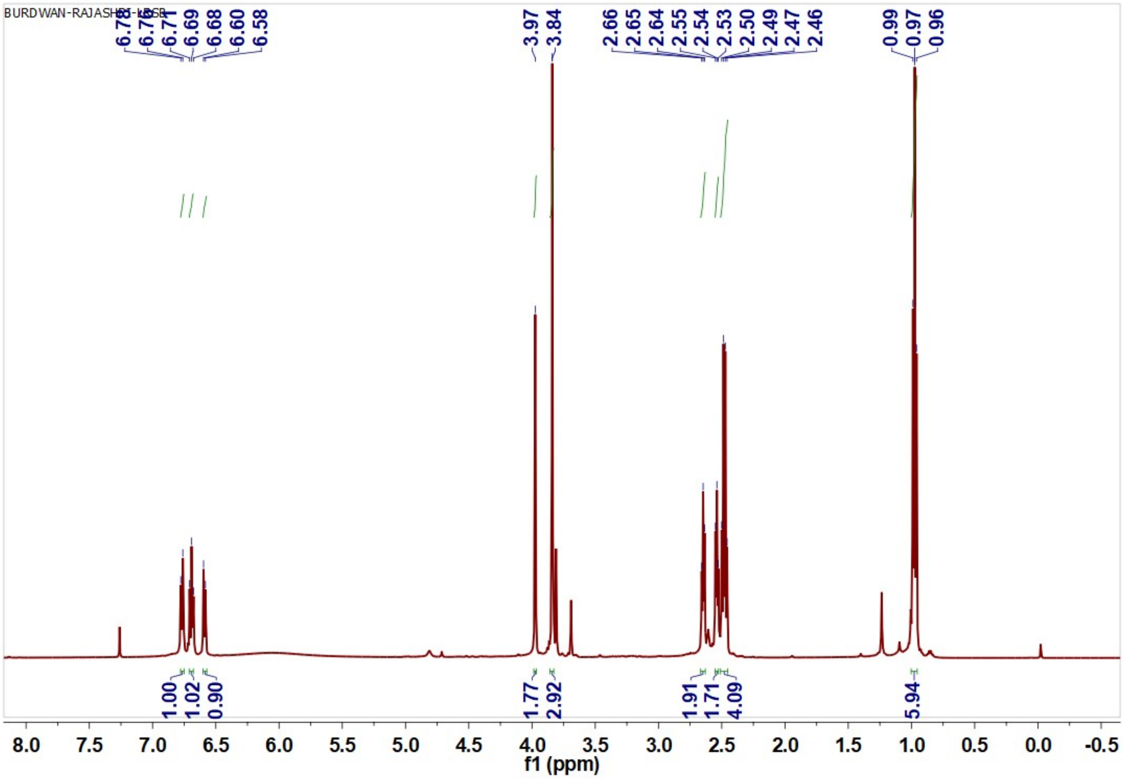

Fig. S1: ^{1}H NMR spectrum of **MDAMP** (500 MHz, $CDCl_3$).

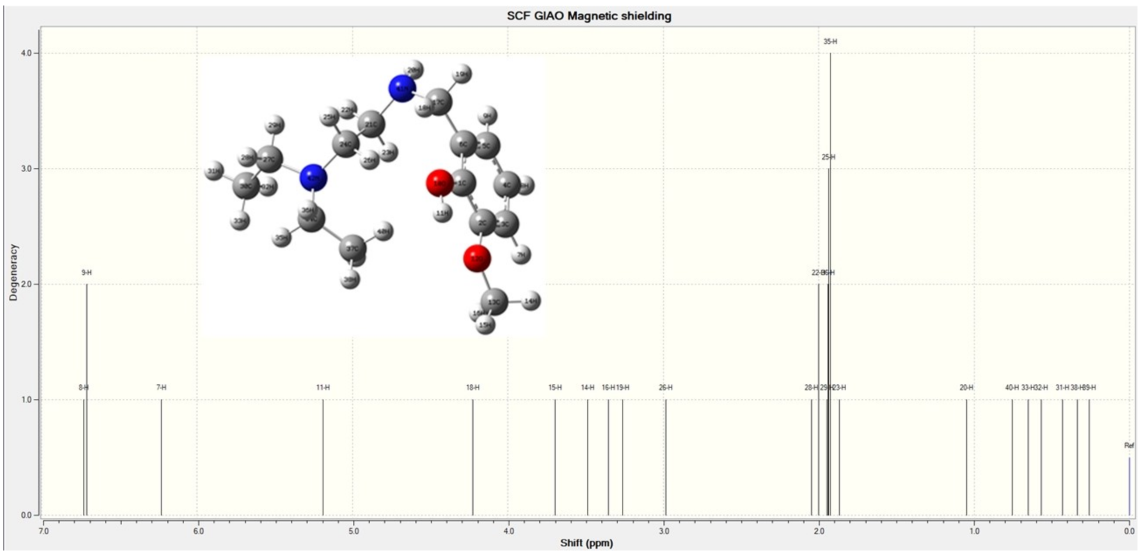

Fig. S2: Simulated ^{1}H NMR spectrum of **MDAMP** obtained using CAM-B3LYP theoretical model and 6-31+G* basis set with fitting set Def2TZV.

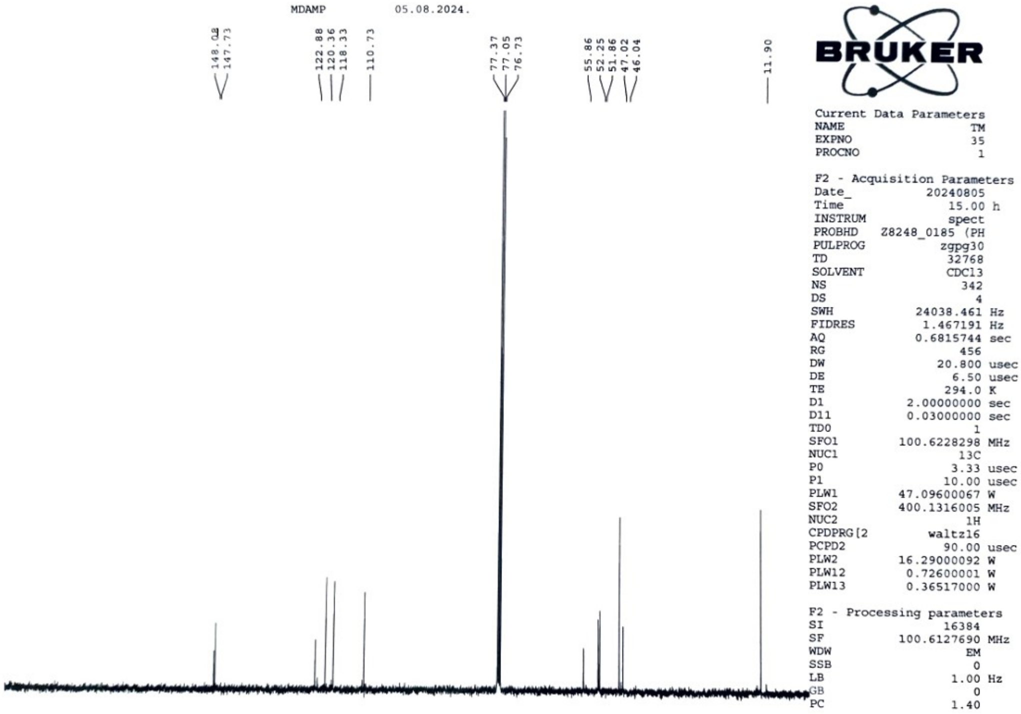

Fig. S3: ^{13}C NMR of **MDAMP**.

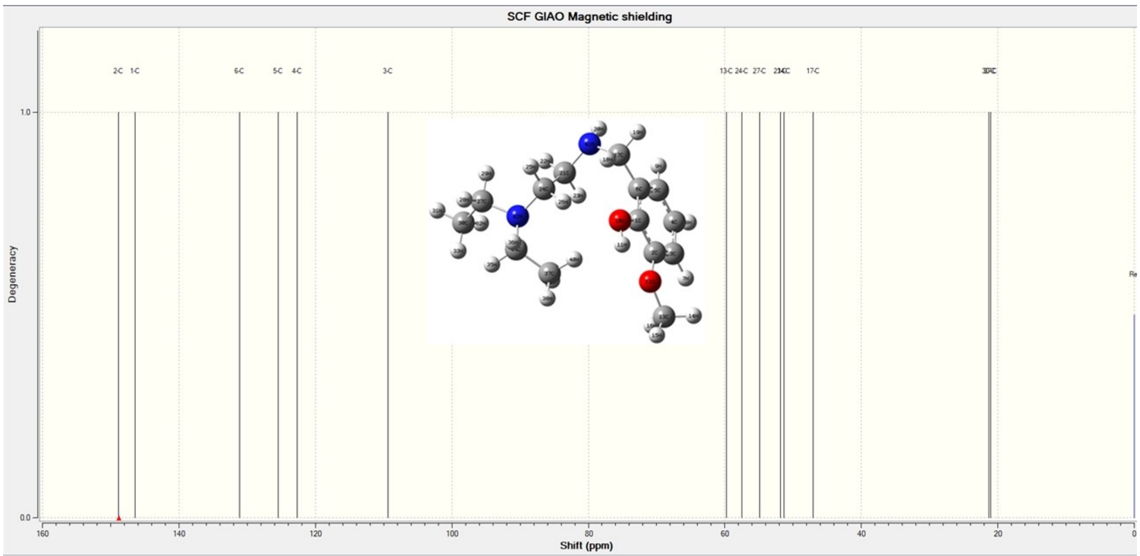

Fig. S4: Simulated ^{13}C NMR of **MDAMP** obtained using CAM-B3LYP theoretical model and 6-31+G* basis set with fitting set Def2TZV.

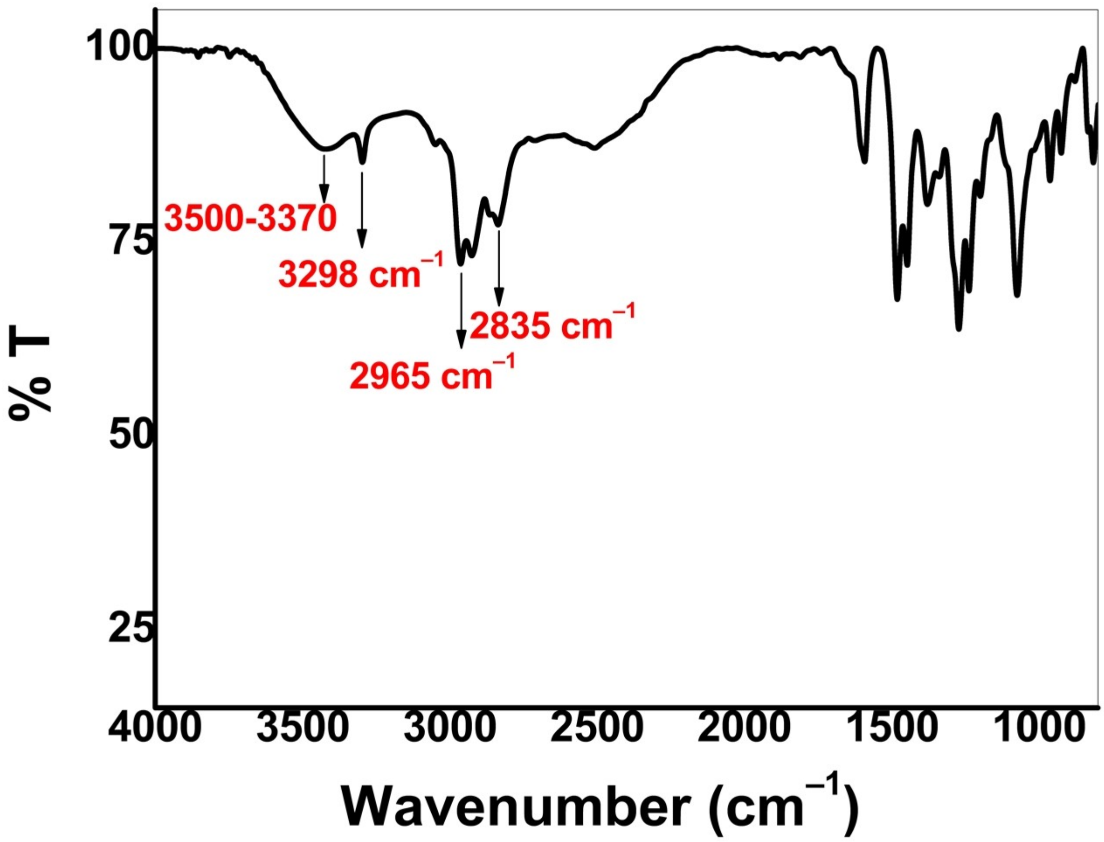

Fig. S5: Experimental IR spectrum of **MDAMP**.

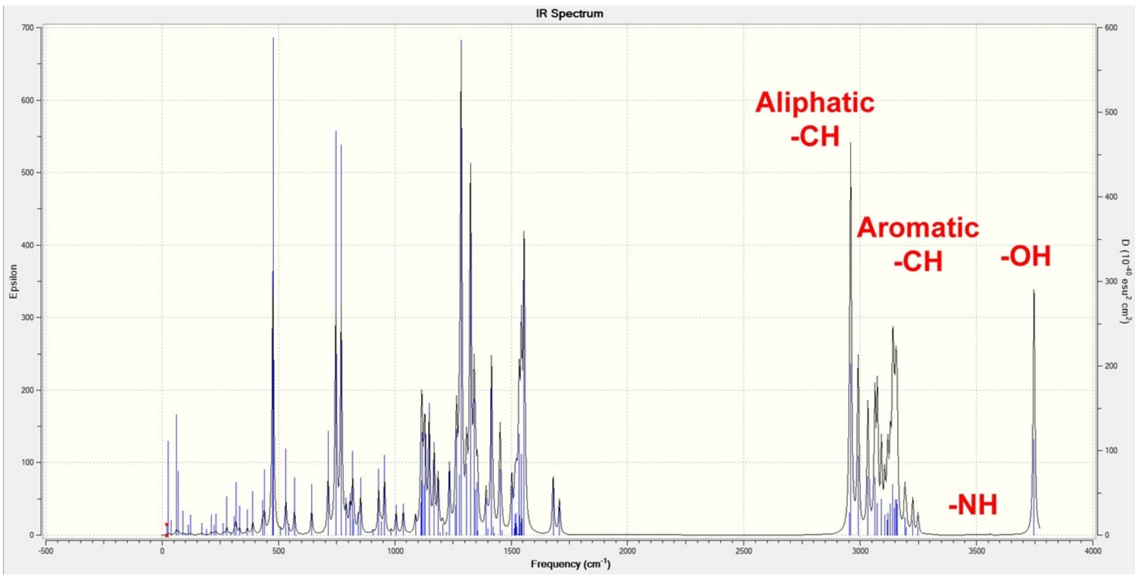

Fig. S6: Simulated IR spectrum of **MDAMP** obtained using CAM-B3LYP theoretical model and 6-31+G* basis set with fitting set Def2TZV.

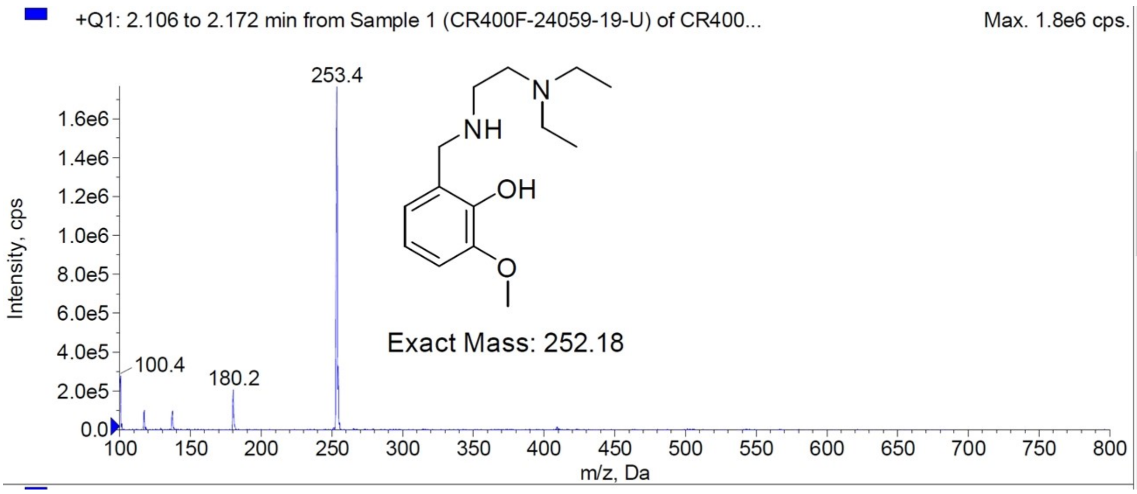

Fig. S7: Mass spectrum of **MDAMP**.

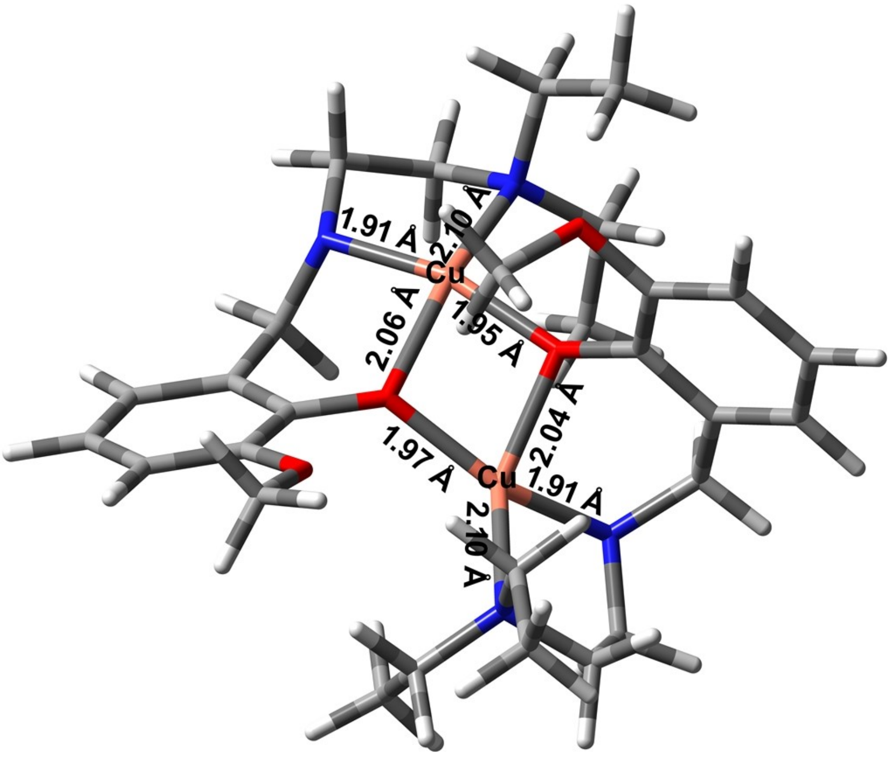

Fig. S8: Optimized structure of **MDAMP-Cu^{2+}** (1:1) complex in vacuum.

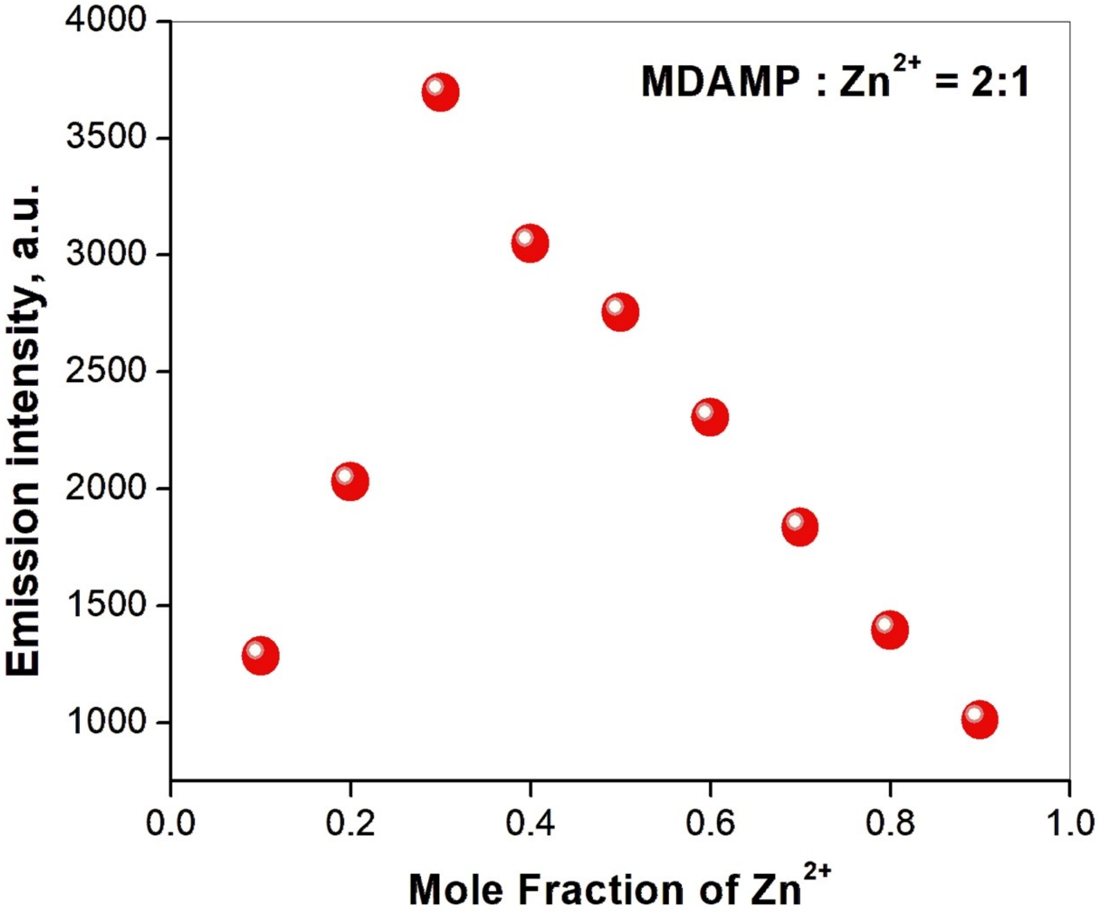

Fig. S9: Job's plot between **MDAMP** and ZnP from variation of emission intensity at 325 nm vs mole fraction of ZnP.

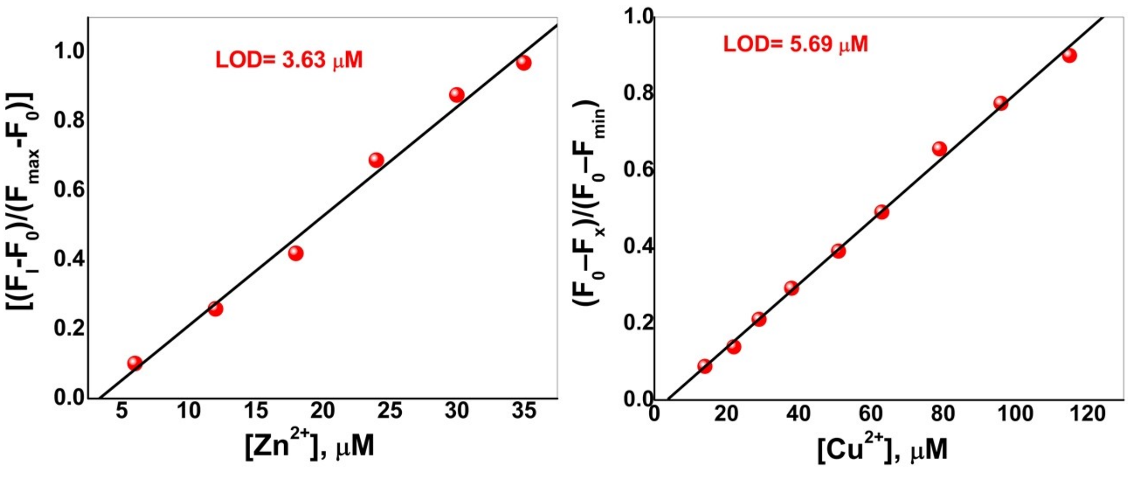

Fig. S10. Calculation of limit of detection plot for Zn^{2+} (left) and LOD plot for Cu^{2+} (right), where [**MDAMP**]= 80μM, Temp. 298K in ACN.

Table S2: Z-coordinate values for the optimized structure of **MDAMP** obtained using CAM-B3LYP theoretical model and 6-31+G* basis set with fitting set Def2TZV.

C	-1.02412000	-0.41520600	0.32269000
C	0.35505100	-0.65745500	0.44621700
C	1.26810800	0.11238400	-0.25739700
C	0.79651600	1.13506100	-1.08732900
C	-0.56485400	1.37053500	-1.20226000
C	-1.50063700	0.59564000	-0.50265100
H	2.33281200	-0.06781000	-0.16659500
H	1.50640800	1.74699300	-1.63498000
H	-0.92202700	2.17424800	-1.84175000
O	-1.89653400	-1.19106700	1.03329100
H	-1.37576600	-1.83161400	1.54852400
O	0.65822500	-1.68409800	1.29581000
C	2.02619300	-2.01660700	1.49510000
H	2.57367600	-1.16955700	1.92066100
H	2.03360500	-2.84879800	2.19782000
H	2.49177700	-2.32462300	0.55346300
C	-2.98786200	0.85408700	-0.66095300
H	-3.53054100	0.42743600	0.18486700
H	-3.16072100	1.93483800	-0.63806500
H	-3.14136100	0.80908500	-2.69168500
C	-3.54566200	-1.09643400	-2.09437200
H	-3.73275900	-1.28413700	-3.15598600
H	-2.55886400	-1.52676600	-1.86237100
C	-4.60067800	-1.81435400	-1.25319700
H	-5.57928400	-1.32257500	-1.39845600
H	-4.34273200	-1.70264900	-0.19792900
C	-5.50745500	-3.48624000	-2.74642600
H	-6.58010300	-3.44995700	-2.47851000
H	-5.34099300	-2.66652800	-3.45066500
C	-5.18864100	-4.79855200	-3.45287200
H	-5.83370500	-4.92016000	-4.32977900
H	-4.14641300	-4.80963900	-3.78789900
H	-5.34527200	-5.66720700	-2.80590200
C	-5.14795200	-4.02120200	-0.41256800
H	-5.48821600	-4.99341700	-0.77850900
H	-6.03017600	-3.53654000	0.04635300
C	-4.07091500	-4.25202900	0.64019800
H	-4.47963200	-4.82790300	1.47773000
H	-3.23312700	-4.81274800	0.21282500

H	-3.67835100	-3.31254600	1.04015200
N	-3.58999100	0.35309700	-1.90226200
N	-4.67880700	-3.24302300	-1.56200700

1 2 1.5 6 1.5 10 1.0
2 3 1.5 12 1.0
3 4 1.5 7 1.0
4 5 1.5 8 1.0
5 6 1.5 9 1.0
6 17 1.0
7
8
9
10 11 1.0
11
12 13 1.0
13 14 1.0 15 1.0 16 1.0
14
15
16
17 18 1.0 19 1.0 41 1.0
18
19
20 41 1.0
21 22 1.0 23 1.0 24 1.0 41 1.0
22
23
24 25 1.0 26 1.0 42 1.0
25
26
27 28 1.0 29 1.0 30 1.0 42 1.0
28
29
30 31 1.0 32 1.0 33 1.0
31
32
33
34 35 1.0 36 1.0 37 1.0 42 1.0
35
36
37 38 1.0 39 1.0 40 1.0
38

39

40

41

42

Table S3: Z-coordinate values for the simulated IR frequency of **MDAMP** obtained using CAM-B3LYP theoretical model and 6-31+G* basis set with fitting set Def2TZV.

C	-1.01530000	-0.42758900	0.29301300
C	0.36354200	-0.65154700	0.43557300
C	1.27947400	0.15873100	-0.21549100
C	0.81059500	1.20654500	-1.01297200
C	-0.55130200	1.42359300	-1.14720400
C	-1.48954400	0.60772600	-0.50238200
H	2.34494400	-0.00875500	-0.10904900
H	1.52139500	1.85199400	-1.51924000
H	-0.90832500	2.24860200	-1.75939700
O	-1.89018000	-1.24140800	0.95185600
H	-1.37068800	-1.89725900	1.44613700
O	0.66686100	-1.70957300	1.25244900
C	2.02934600	-2.02943000	1.45991100
H	2.56056600	-1.19451500	1.93102600
H	2.04005100	-2.89125000	2.12716600
H	2.51832500	-2.29151400	0.51472100
C	-2.97752600	0.84221300	-0.69010300
H	-3.52800600	0.41898600	0.15252600
H	-3.16685200	1.92092400	-0.68187900
H	-3.09460800	0.75914600	-2.72320100
C	-3.52520700	-1.13455400	-2.09235300
H	-3.69686600	-1.34087200	-3.15369200
H	-2.55541000	-1.58583900	-1.83238800
C	-4.61480500	-1.81308900	-1.26274900
H	-5.57561000	-1.29615600	-1.43518200
H	-4.37371000	-1.69176600	-0.20454000
C	-5.53294200	-3.49659200	-2.73848500
H	-6.61025200	-3.46397000	-2.48433200
H	-5.36435300	-2.67980400	-3.44624900
C	-5.19754200	-4.81147200	-3.43338000
H	-5.82234800	-4.94092500	-4.32413400
H	-4.14688500	-4.82093500	-3.73915600
H	-5.36589900	-5.67727200	-2.78536900
C	-5.17471500	-4.01158300	-0.39969500

H	-5.51663800	-4.98682300	-0.75756700
H	-6.05433600	-3.52800600	0.06799700
C	-4.08558600	-4.23603300	0.64256600
H	-4.47931700	-4.81659400	1.48450600
H	-3.24783900	-4.78442000	0.20049100
H	-3.69874400	-3.29198400	1.03694000
N	-3.54986800	0.31730000	-1.93064700
N	-4.71567600	-3.24227100	-1.55371700

1 2 1.5 6 1.5 10 1.0

2 3 2.0 12 1.0

3 4 1.5 7 1.0

4 5 2.0 8 1.0

5 6 1.5 9 1.0

6 17 1.0

7

8

9

10 11 1.0

11

12 13 1.0

13 14 1.0 15 1.0 16 1.0

14

15

16

17 18 1.0 19 1.0 41 1.0

18

19

20 41 1.0

21 22 1.0 23 1.0 24 1.0 41 1.0

22

23

24 25 1.0 26 1.0 42 1.0

25

26

27 28 1.0 29 1.0 30 1.0 42 1.0

28

29

30 31 1.0 32 1.0 33 1.0

31

32

33

34 35 1.0 36 1.0 37 1.0 42 1.0

35

36

37 38 1.0 39 1.0 40 1.0

38

39

40

41

42

Table S4: Z-coordinate values for the simulated ^{1}H and ^{13}C NMR of **MDAMP** obtained using CAM-B3LYP theoretical model and 6-31+G* basis set with fitting set Def2TZV.

C	-1.44396800	-0.28154900	0.48905300
C	-0.17660600	-0.86266800	0.62162100
C	0.82484600	-0.59811400	-0.29687300
C	0.54405500	0.25930500	-1.36886800
C	-0.71794400	0.82104000	-1.50308500
C	-1.73664400	0.55723200	-0.57578600
H	1.80332100	-1.04313900	-0.19661100
H	1.31641800	0.47388600	-2.09264900
H	-0.93797100	1.46667600	-2.34378100
O	-2.41938500	-0.58564300	1.42894600
H	-2.04817200	-1.17663400	2.10852000
O	-0.07168200	-1.70498900	1.72738700
C	1.16306800	-2.42258400	1.92139700
H	1.98819900	-1.72886600	2.08639100
H	1.01318500	-3.03398200	2.80332000
H	1.37708600	-3.05653700	1.06008300
C	-3.14014300	1.10145100	-0.77586800
H	-3.75412300	0.81557500	0.07538200
H	-3.11455100	2.19159300	-0.79885500
H	-3.52916500	1.20891200	-2.81832800
C	-3.72082100	-0.79170400	-2.29005000
H	-4.20534000	-0.97290300	-3.25112900
H	-2.69446700	-1.17719500	-2.36072600
C	-4.43465100	-1.60117600	-1.21013400
H	-5.45983100	-1.22235000	-1.09320400
H	-3.93066700	-1.45701000	-0.25330600
C	-5.54458700	-3.45844300	-2.38411300
H	-6.41413300	-3.72933400	-1.76270400
H	-5.84738700	-2.60274300	-2.98957500

C	-5.17590200	-4.61262200	-3.31207700
H	-6.02201500	-4.88925900	-3.94267400
H	-4.34170700	-4.31536000	-3.94592500
H	-4.87366200	-5.49720000	-2.75126900
C	-4.13187000	-3.91966800	-0.41386200
H	-4.37312800	-4.93885600	-0.71762600
H	-4.78054500	-3.68074400	0.44498400
C	-2.66438900	-3.85877500	0.00227200
H	-2.46109900	-4.55990600	0.81360900
H	-2.03491200	-4.10801400	-0.85108800
H	-2.39284200	-2.86099500	0.34508400
N	-3.78347400	0.64660800	-2.01691700
N	-4.41416900	-3.03135200	-1.54863800

1 2 1.5 6 1.5 10 1.0

2 3 2.0 12 1.0

3 4 1.5 7 1.0

4 5 1.5 8 1.0

5 6 1.5 9 1.0

6 17 1.0

7

8

9

10 11 1.0

11

12 13 1.0

13 14 1.0 15 1.0 16 1.0

14

15

16

17 18 1.0 19 1.0 41 1.0

18

19

20 41 1.0

21 22 1.0 23 1.0 24 1.0 41 1.0

22

23

24 25 1.0 26 1.0 42 1.0

25

26

27 28 1.0 29 1.0 30 1.0 42 1.0

28

29

30 31 1.0 32 1.0 33 1.0

31

32

33

34 35 1.0 36 1.0 37 1.0 42 1.0

35

36

37 38 1.0 39 1.0 40 1.0

38

39

40

41

42

Reference

S1. V. Luxami and S. Kumar, ESIPT based dual fluorescent sensor and concentration dependent reconfigurable boolean operators, *RSC Adv.*, 2012, **2**, 8734−8740.

S2. A. Hens and K. K. Rajak, Selective fluorometric detection of F^- and Zn(ii) ions by a N, O coordinating sensor and naked eye detection of Cu(ii) ions in mixed-aqueous solution, *RSC Adv.,* 2015, **5**, 44764−44777.

S3. A. Gogoi, S. Samanta and G. Das, A benzothiazole containing CHEF based fluorescence turn-on sensor for Zn2+ and Cd2+ and subsequent sensing of $H_2PO_4^-$ and $P_4O_7^{4-}$ in physiological pH, *Sens. Actuators, B,* 2014, **202**, 788−794.

S4. A. Kundu, P. S. Hariharan, K. Prabakaran and S. P. Anthony, Synthesis of new Colori/fluorometric chemosensor for selective sensing of biologically important Fe^{3+}, Cu^{2+} and Zn^{2+} metal ions, *Spectrochim. Acta, Part A,* 2015, **151**, 426−431.

S5. D. Sarkar, A. K. Pramanik and T. K. Mondal, A novel coumarin based molecular switch for dual sensing of Zn(ii) and Cu(ii), *RSC Adv.,* 2015, **5**, 7647−7653.

S6. S. N. Ansari, A. K. Saini, P. Kumari and S. M. Mobin, An imidazole derivative-based chemodosimeter for Zn^{2+} and Cu^{2+} ions through "ON–OFF–ON" switching with intracellular Zn^{2+} detection, *Inorg. Chem. Front.,* 2019, **6**, 736−745.

S7. H. Singh, G. Bhargava, S. Kumar and P. Singh, Quadruple-signaling (PET, ICT, ESIPT, C N rotation) mechanism-based dual chemosensor for detection of Cu 2+ and Zn 2+ ions: TRANSFER, INH and complimentary OR/NOR logic circuits, *J. Photochem. Photobiol. A*, 2018, **357**, 175−184.

S8. H.-W. Zheng, Y. Kang, M. Wu, Q. -F. Liang, J.-Q. Zheng, X.-J. Zheng and L.-P. Jin, ESIPT-AIE active Schiff base based on 2-(2′-hydroxyphenyl) benzo-thiazole applied as multi-functional fluorescent chemosensors, *Dalton Trans.,* 2021, **50**, 3916−3922.

S9. J. S. Ganesan, S. Gandhi, K. Radhakrishnan, A. Balasubramaniem, M. Sepperumal and S. Ayyanar, Execution of julolidine based derivative as bifunctional chemosensor for Zn^{2+} and Cu^{2+} ions: Applications in bio-imaging and molecular logic gate, *Spectrochim. Acta, Part A*, 2019, **219**, 33−43.

S10. P. Yadav, S. Gond, A. Shekher, S. C. Gupta, U. P. Singh and V. P. Singh, A multifunctional basic pH indicator probe for distinguishable detection of Co^{2+}, $Cu^{2+}$and $Zn^{2+}$with its utility in mitotracking and monitoring cytoplasmic viscosity in apoptotic cells, *Dalton Trans.,* 2022, **51**, 6927−6935.

S11. H. Liu, S. Ding, Q. Lu, Y. Jian, G. Wei and Z. Yuan, A versatile Schiff base chemosensor for the determination of trace Co^{2+}, Ni^{2+}, Cu^{2+}, and Zn^{2+} in the water and its bioimaging applications, *ACS Omega*, 2022, **7**, 7585−7594.

S12. L. Zhang, X. Zhu, J. Li, Y. Li, H. Huang and Y. Gao, A coumarin-based fluorescent probe for sequential recognition of zinc ion and nitric oxide, and its applications in real water sample, fluorescence anti-counterfeiting and bioimaging in vivo, *Spectrochim. Acta, Part A*, 2025, **341**, 126405.

S13. J. Chen, S. Liu, D. Deng, G. Guo and Y. Min, A highly-sensitive fluorescent probe for the detection of copper ions and its applications in water quality monitoring, neural cell imaging and plant imaging, *Spectrochim. Acta, Part A*, 2025, **329**, 125613.

S14. M. Zhang and C. Tong, Dual-response fluorescent probe for simultaneously detecting HOCl and Zn^{2+} in environmental water samples and evaluating the oxidative stress in the zebrafishes induced by pollutants via fluorescence imaging *Sensors and Acuators B*, 2024, **409**, 135617.

S15. P. Wei, L. Xiao, Y. Gou, F. He, D. Zhou, Y. Liu, B. Xu, P. wang and Y. Zhou, Fluorescent "on–off–on" probe based on copper peptide backbone for specific detection of Cu (II) and hydrogen sulfide and its applications in cell imaging, real water samples and test strips, *Microchem. Journal*, 2022, **182**, ,107848.

S16. H. Sun, Q. Xu, C. Xu, Y. Zhang, J. Ai, M. Ren, K. Liu and F. Kong, Construction of a water-soluble fluorescent probe for copper (II) ion detection in live cells and food products, *Food Chemistry*, 2023, **418**, 135994.

S17. L. Xie, R. Zheng and L. Li, A multifunctional fluorescent probe based on octupolar conjugated merocyanine dyes for the rapid and sensitive detection of copper (II) and nitrite in aquaculture water and food samples, *Dyes and Pigments*, 2022, **203**, 110374.

S18. P. K. Giri, S. S Samanta, M. Shyamal, S. Mandal, S. Barman and A. Misra, Fluorescence 'turn-on' dual sensor for the selective detection of Al^{3+} and Zn^{2+} and the use of AI-based soft computing to predict machine learning outcomes, *New J. Chem.*, 2025, **49**, 14646-14658.

S19. S. Paul, A. R. Choudhury, and N. Dey, Dual-Mode Multiple Ion Sensing via Analyte-Specific Modulation of Keto−Enol Tautomerization of an ESIPT Active Pyrene Derivative: Experimental Findings and Computational Rationalization, *ACS Omega,* 2023, **8**, 6349−6360.